

Analysis of Excited Species Formation across the Flame of Various Ammonia-Hydrogen Fired Combustor Geometries

Marco Osvaldo Viguera-Zuniga, Maria Elena Tejeda del Cueto, Jordan Davies, Syed Mashruk, and Agustin Valera-Medina*

Although ammonia can be used as a fuel, it also presents drawbacks that require further investigation before the chemical can overtake fossil fuels in combustion systems. The main barriers are the low flammability in combination with high NO_x emissions. Although the first barrier can be surpassed by doping ammonia with hydrogen, the second becomes more challenging under these conditions, as hydrogen increases NO emissions due to the increase in H radicals in the chemical pool of species. How the change in radicals impacts the stability of the flame, its reactivity, and emissions profile is of the greatest concern for the use of these net zero fuels. Thus, the work herein presented shows the trends of excited species such as NH*, NH₂*, and OH* when using ammonia–hydrogen at 70%–30% (vol) blending. Various equivalence ratios are employed from lean to rich conditions. Results denote that there is a continuous displacement of radicals across the field, with NH₂* relocating closer to the centerline of the burner as equivalence ratio increases, while NH* tends to raise its location while dislocating from the production/consumption of OH* radicals. The results can be used to target desirable radicals for the mitigation of emissions and flame control.

emissions. However, renewables suffer from intermittency issues that can only be solved via storage. From batteries to chemicals, the latter offer both the largest capacity and the longest periods of storage.^[1] Out of these chemicals, hydrogen has been extensively promoted as the preferred chemical to decarbonize the global economy. Various methods of hydrogen storage have been assessed with particular emphasis on liquid hydrogen (LH₂), liquid organic hydrogen carriers, and ammonia (NH₃), among others. As an example and for comparison, the Hydrogen Council^[2] presented a comparison between these vectors to distribute hydrogen from locations with high renewable potential to those where large consumption of the molecule was imminent, **Figure 1**. The results show that of hydrogen via these methods is relatively similar. However, further attention needs to be paid to ammonia, where a large cracking component of 0.9 to 1.6

1. Introduction

Global demand for energy will considerably increase in the following decades with faster industrialization and greater population increase in developing economies. The problem is linked to a greater carbon footprint consequence of the human activity this will generate. Therefore, governments, industries, and institutions of all kinds have turned to the development of new technologies that employ renewable energy capable of mitigating these carbon


USD/kg_{H₂} dwarfs the costs of ammonification and shipping. Thus, if cracking was not included and direct combustion of the chemical was employed, the best option to move hydrogen both through long distances and long periods would be ammonia.

It is for that reason that considerable work has now started to take place in the direct use of ammonia. One important contender in the use of the chemical is gas turbines for power generation. Initial works performed in the 1960s by Verkamp et al.^[3] Pratt,^[4] and Newhall and Starkman^[5] showed the potential of the chemical for such an application, with the U.S. Army and Solar Division of International Harvester Company recommending through a dedicated program the progression in the technology to mitigate emissions and improve combustion performance. Unfortunately, the era of accessible oil and gas stopped any further interest on the use of ammonia.

Decades would pass, and it would be the work from Toyota Energy Solutions Inc. in collaboration with Tohoku University and the National Institute of Advanced Industrial Science and Technology (AIST) of Japan that in 2016 would reconvert a 50 and 300 kW micro gas turbines to operate with ammonia and ammonia blends.^[6] The development was simultaneous to work conducted in Wales, Saudi Arabia, and Norway to understand the complexities of ammonia and ammonia blends in a variety of gas turbine representative configurations.^[7] These studies opened series of scientific questions still unresolved. Among the great

M. O. Viguera-Zuniga, M. E. Tejeda del Cueto
School of Engineering
Universidad Veracruzana
94294 Veracruz, Mexico

J. Davies, S. Mashruk, A. Valera-Medina
College of Physical Sciences and Engineering
Cardiff University
Cardiff CF24 3AA, UK
E-mail: valeramedina1@cardiff.ac.uk

 The ORCID identification number(s) for the author(s) of this article can be found under <https://doi.org/10.1002/ente.202401404>.

© 2024 The Author(s). Energy Technology published by Wiley-VCH GmbH. This is an open access article under the terms of the Creative Commons Attribution License, which permits use, distribution and reproduction in any medium, provided the original work is properly cited.

DOI: 10.1002/ente.202401404

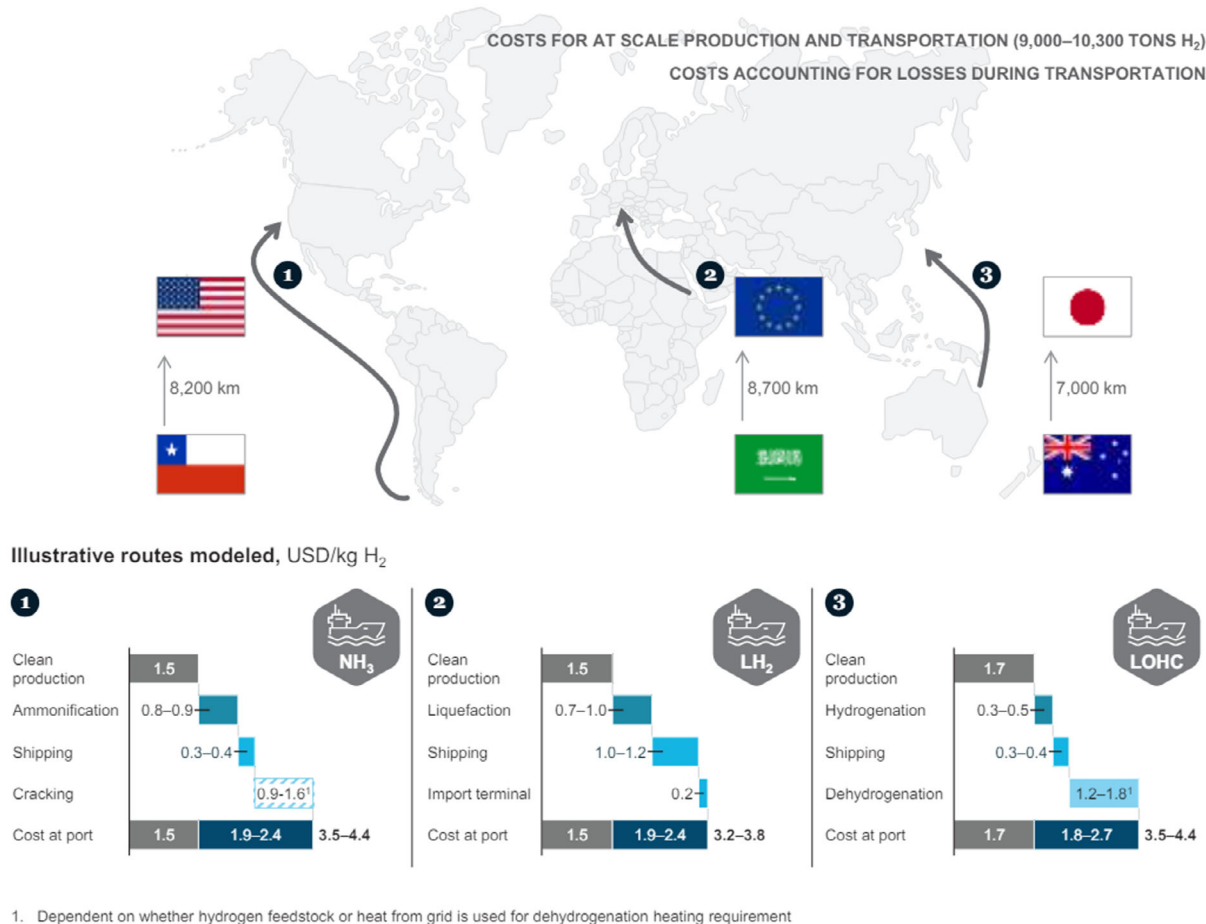


Figure 1. Hydrogen cost from production to port depending on vector employed for its storage and distribution. Courtesy of the Hydrogen Council.^[2]

variety of inquiries, one that has received less attention is the characterization of excited radicals as ammonia is burned.

Chemiluminescence-based diagnostics techniques have been widely used for combustion measurements in laboratory and industrial applications,^[8] providing a noninvasive and sensitive method for measuring combustion characteristics, due to its cost-efficient and simple set-up. The first recorded campaign for excited radical analyses using chemiluminescence was published by Viguera-Zuniga et al.^[9] who performed a thorough analysis of the formation of various species within a combustor operating with ammonia blends. The work elucidated the position of various excited radicals (NH₂^{*}, NH^{*}, and OH^{*}) and their progression based on equivalence ratio and hydrogen/methane content. At the time, it was unclear if the doping agents were leading to a constant, well-defined repositioning of the flame. Further computational fluid dynamics analyses showed the impact of hydrogen/ammonia, while also emphasizing the acute interaction between radicals such as NH₂, NH, or OH in the context of NO formation and flame location. According to other studies,^[10,11] it appeared that a reduction of emissions was caused at the postflame zone which suffers an increase in reactivity in the reactions NH₂ + NO → NNH + OH and NH₂ + NO → N₂ + H₂O and a decay in the producing reaction N + OH → NO + H at the flame front under particular circumstances such as higher

equivalence ratios and moderate hydrogen content. Vast literature on the subject exists behind NH_x impacts on NO_x formation.^[12–15]

Further fundamental analyses progressed to characterize emissions and reaction kinetic impacts of these radicals. Mashruk et al.^[10] performed series of experimental and numerical analyses to determine the progression of NO_x species in ammonia/hydrogen blends. Results showed not only change in spectral signatures of the blends at various equivalence ratios but also the change in location of NH^{*} and NH₂^{*} species across different ammonia contents. It was found that that NH₂^{*} tends to raise toward the combustor outlet as equivalence ratio increases with the acute mitigation of NO emissions. The study was complemented by Mashruk et al.^[16] who depicted the clear impact of NH, NH₂, and OH radicals—with high correlation to NH^{*}, NH₂^{*}, and OH^{*} experimental signatures—in modeled heat release and laminar burning velocities of ammonia/hydrogen blends. Recent works have been conducted by Karan et al.^[17] who evaluated NH₂^{*} signatures in the curvature of ammonia-fed flames under perturbed conditions. The results permitted visualize the effect caused by the Lewis number, concluding that under rich equivalence ratios and Le > 1, the negative curvature promoted the production of hydrogen leading to local enhancement in reactivity, and changes in local thickness. Recent works done by Suarez et al.^[18] also showed how the change in NH₂^{*} in

an ammonia/hydrogen flame was positively correlated to the oxygen levels of the blend. Additional tests that correlate NH_2^* , NH^* , and OH^* species have been used to establish clear relationships that identify the operating conditions of ammonia flames under laminar^[19] and turbulent^[20] regimes. Zhu et al.^[19] measured the chemiluminescence spectra of laminar premixed NH_3/CH_4 flames for various equivalence ratios ($0.60 \leq \phi \leq 1.30$), NH_3 fuel fractions and strain rates ($55 \text{ s}^{-1} \leq \alpha \leq 300 \text{ s}^{-1}$). They identified the relevant excited radicals, including NO^* , OH^* , NH^* , CN^* , CH^* , and CO^* , and examined the relationship between chemiluminescence intensity ratios and the flames' inlet conditions. The results denoted that excited radical trends follow equivalence ratios and ammonia fractions, while by normalizing the results some correlations were linear and with potential of being used for further control purposes. Similarly, Mashruk et al.^[20] showed that under turbulent conditions ($10\,000 \leq \text{Re} \leq 40\,000$) these trends persist, opening the possibility of using artificial intelligence methods to ensure stable air/fuel feeding for temperature, flame stability, and emissions control. Studies using two-line chemiluminescence techniques are expanding from the use of fossil fuels^[21] to alternative blends, even expanding into novel reaction mechanisms that also include these excited species. Of particular interest is the work from Konnov^[22] whose latest model (2023) expands from previous works and includes the formation and consumption of excited NO_2^* , NO(A) , NH^* , and NH_2^* , hence showing the high relevance of the topic within the combustion community working on ammonia blends.

Experimental trials attempting the use of more complex blends have also denoted how NHx^* and OH^* radicals can have a critical impact on emissions performance. Studies performed by Pugh et al.^[23] evaluate the production of N_2O emissions from humidified ammonia–hydrogen blends at pressures up to 0.23 MPa, lean equivalence ratios (≈ 0.5), and $\approx 5.4\%$ humidification. Results show a decrease of emissions with pressure (from ≈ 200 to ≈ 30 ppm and from 0.00 to 0.23 MPa) as a consequence of the increase reactivity of $\text{N}_2\text{O(+M)} \rightarrow \text{N}_2 + \text{O(+M)}$. Simultaneously, changes in the operating conditions (i.e., consequence of additional water) lead to a boost in OH^* and NH_2^* , which due to the lean conditions, also delivered greater quantities of N_2O due to the increase in reactivity of $\text{NH} + \text{NO} \rightarrow \text{N}_2\text{O} + \text{H}$. Fortunately, pressure had a direct impact on both NO and N_2O under these humidified conditions, with reduction of these emissions in two and four times, respectively. The close relationship between combustion characteristics and chemiluminescence allows to better understand the combustion process to optimize reactive systems for efficiency and emissions reduction. This point was recently raised by Weng et al.^[24] who picked up chemiluminescence spectra showing an increase of NO_2^* under lean ammonia combustion, while NH_2^* was the dominant species at rich conditions. However, their intensity maps only denote the change of species across various equivalence ratios, without further details on the location of these radicals across the flame front.

Therefore, the impact of these excited radicals is still barely addressed in most available literature. Further work is necessary to understand their interactions, especially for flame stability and emissions abatement purposes. The technique, with great potential in gas turbines^[25] and internal combustion engines,^[26] can be employed not only for combustion enhancement but also as a

robust control strategy. Therefore, the objective of this work is to present an analysis that provides evidence of the progression of these excited radicals across the flame under different operating conditions (i.e., equivalence ratios), geometries, and power regimes. By knowing the position of radicals across the flame it is possible to target areas of high radical density through stratification or advanced injection methods, hence maximizing the recombination of certain species before they oxidize or convert into radicals with different properties. This is particularly critical for species such as NH_2 and NH whose reaction paths can lead to the formation of molecular nitrogen or nitrogen oxides, respectively.

2. Methodology

A couple of tangential swirl burners with different nozzles were employed at 8 and 10 kW power, respectively, and 1.05 swirl, as shown in **Figure 2**. The first unit, MK1, uses a simple nozzle that delivers the fuel into a plenum after a short, 15 mm elongation nozzle. In contrast, the second unit, NIK17, delivers the fuel using a more complex nozzle which protrudes into a Coanda plate to form an external recirculation zone that enhances post-combustion recombinations in such a zone, **Figure 3**. To avoid flashback, the central injector widens, hence increasing Re and avoiding the movement of the flame back into the system. Both units were fed using Bronkhorst mass flow controllers that enabled a precision of 0.5% within the 15%–95% range of the mass flow rate. The units were fed using hydrogen and ammonia blended at 70–30 (%vol) NH_3/H_2 . The rationale of using two different nozzle geometries and different powers was to test the theory behind the radical localization removing both nozzle geometrical and power rates dependencies. It must be emphasized, particularly on the last parameter, that the proposed theory applied to low power rates, and more experiments are required at higher power outputs to test this theory under those conditions. All experiments were conducted at atmospheric pressure and inlet temperature as in **Table 1**.

A pair of LaVision CCD cameras were employed to visualize OH^* , NH^* , and NH_2^* at a frequency of 10 Hz and a gain of 85%. LaVision Davis v10 was used to gather 200 frames per flame, which were then postprocessed using a MatLab script designed to conduct Abel deconvolution averaging. Averaged calibration data were used to determine the radius of the image based on a separation of 10 mm between holes and a colourmap of each image was produced to determine the location of the central pixel column.

All chemiluminescence images were analyzed using a bespoke MatLab program developed to determine the center of intensity (CoI) of each radical,^[9] herein, giving insights of the average movement of the flame, which is compiled and depicted in the results below. Half of each image was used to avoid mirroring. CoI is given by

$$\text{CoI} = \left[\frac{\sum_{i,j} i \cdot I(i,j)}{\sum_{i,j} I(i,j)}, \frac{\sum_{i,j} j \cdot I(i,j)}{\sum_{i,j} I(i,j)} \right] \quad (1)$$

where $I(i,j)$ is the excited radical (OH^* , NH^* , NH_2^*) intensity function. Using this method, the CoI is attracted by those regions with higher-intensity pixels. The background was subtracted from the raw images to give weight only to radical zones.

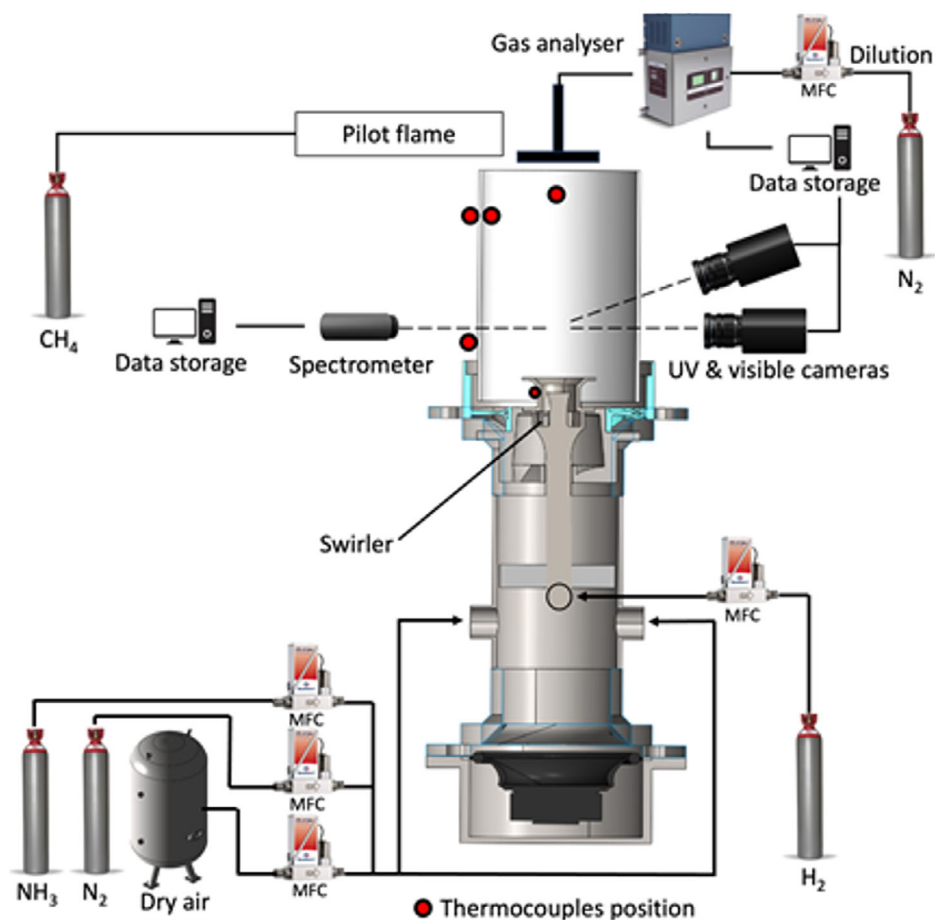


Figure 2. Tangential combustor with measuring techniques and control systems.

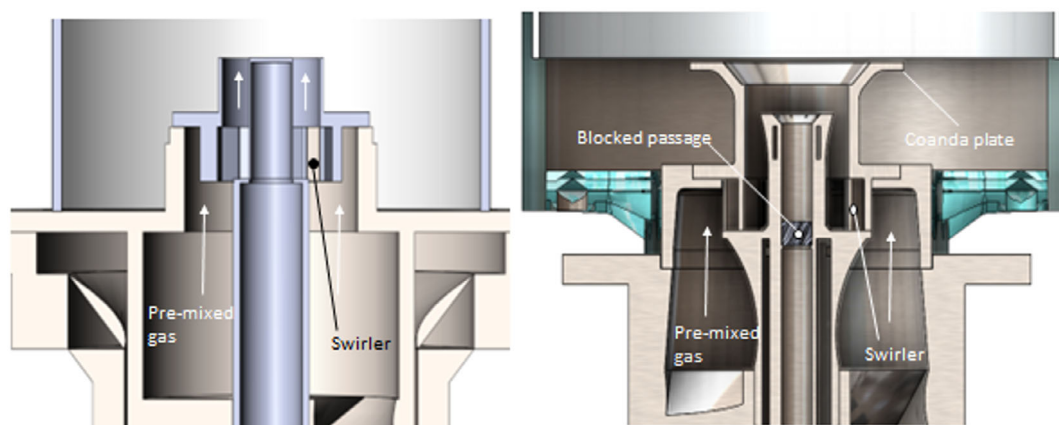


Figure 3. MK1 (left) and NIK17 (right) tangential swirl burners with different nozzles. Premixing is performed in a prechamber in both systems.

Once CoI data were obtained, additional experiments were conducted only using one of the geometries.

Further measurements were done only on MK1 nozzle to determine spectral variations between equivalence ratios. A UV/visible-capable optical fiber head (Stellernet Inc DLENS with

F600 fiber optic cable) was installed 3 cm above the burner's exit and 10 cm away from its central axis. The fiber head was connected to a Stellernet Inc BLUE-Wave spectrometer with a 100 mm focal length and a 25 μm wide entry slit. The spectrometer was equipped with a 600-grooves mm^{-1} grating and a

Table 1. Experimental tests.

Test point	Φ	Power [kW]		NH_3 [g s^{-1}]		H_2 [g s^{-1}]	
		MK1	NIK17	MK1	NIK17	MK1	NIK17
1	0.6	8	10	0.324	0.405	0.016	0.021
2	0.7						
3	0.8						
4	0.9						
5	1						
6	1.1						
7	1.2						
8	1.3						
9	1.4						

Test point	Air [g s^{-1}]		Velocity [m s^{-1}]		Reynolds number	
	MK1	NIK17	MK1	NIK17	MK1	NIK17
1	4.221	–	6.557	–	7540	–
2	3.618	4.516	5.767	11.793	6597	6938
3	3.166	3.951	5.174	10.581	5890	6194
4	2.814	3.512	4.714	9.639	5340	5616
5	2.533	3.161	4.345	8.886	4900	5153
6	2.302	2.874	4.044	8.269	4540	4775
7	2.111	2.634	3.792	7.755	4240	4459
8	1.948	–	3.580	–	3987	–
9	1.809	–	3.397	–	3769	–

Si-CCD detector (Sony ILX511b) featuring 2048 effective pixels of size $14 \times 200 \mu\text{m}^2$, yielding a spectral resolution of 0.5 nm. The detector's exposure time was set to 1 s and 20 scans were averaged to improve the signal-to-noise ratio.

Finally, exhaust emissions (NO , N_2O , NO_2 , NH_3 , O_2 , and H_2O) of the MK1 nozzle were measured using an Emerson CT5100 quantum cascade laser analyzer capable of measuring at 1 Hz ($\pm 1\%$ repeatability, 0.999 linearity). A cross-shaped probe with equispaced holes for homogeneous sample collection was placed 25 mm above the quartz exit to collect the sample gas for analysis. The sample line was heated to prevent condensation, and the measurements were performed at 463 K. 120 points were taken for each test condition and then time-averaged and normalized to 15% O_2 (dry) condition.

3. Results

Results from the campaigns are presented in **Figure 4–9**. The images were not normalized since the intention of the analysis was to determine the CoI of each radical. It must be emphasized that the capture of radicals at the highest equivalence ratios presented technical challenges due to the reduced concentration of some species. To show the decreased intensity of species such as OH^* and NH^* , the brightness increase led to noise next to the quartz walls. The noise was eliminated from the postprocessing steps to ensure only the flame was captured in the analysis.

As depicted in all figures, all exited radicals start appearing close to the bottom of the field of view (where the burner head is located), and as the equivalence ratio increases the flame starts lifting with the radicals located further away from the center. The differences can be observed through the centers of intensity of each intensity profile, **Figure 6** and **7**. However, an interesting phenomenon is that NH_2^* behaves differently to NH^* and OH^* , which follow a more linear progression as they move away from the center of the flow field. In the case of NH_2^* the radical appears spread across the flame even at low equivalence ratios rather than being positioned close to the burner outlet. Furthermore, the location of the radical moves upward without much movement to the sides of the burner, showing how the

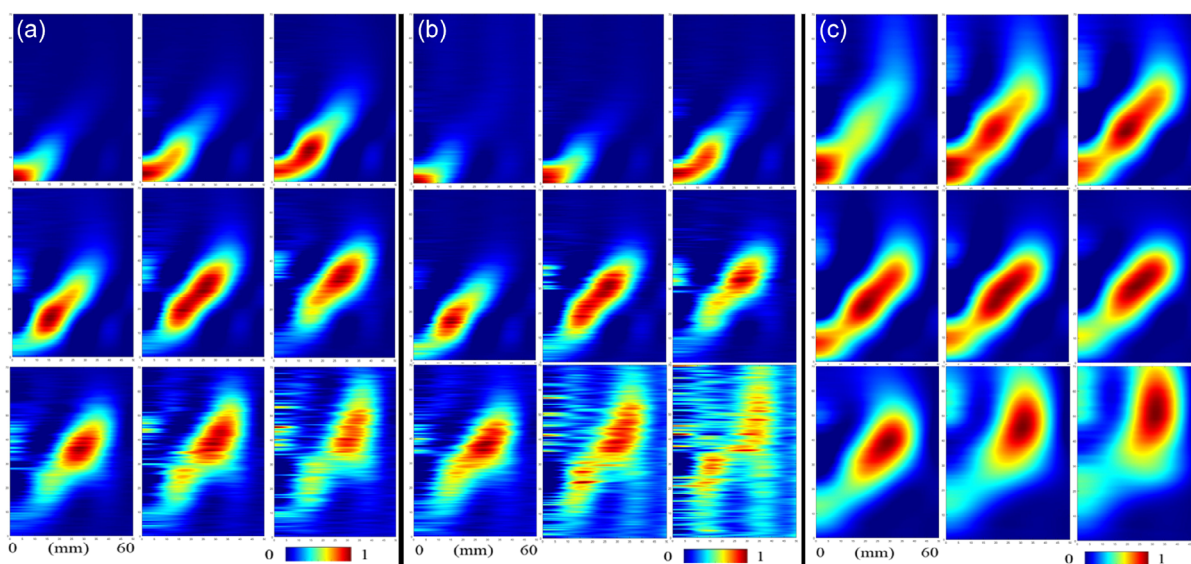


Figure 4. Abel deconvolution of a) OH^* , b) NH^* , and c) NH_2^* intensity profiles from 0.60 to 1.40 ϕ in increments of 0.10 ϕ , from left-top corner to right-bottom corner. Nozzle: MK1. Arbitrary units.

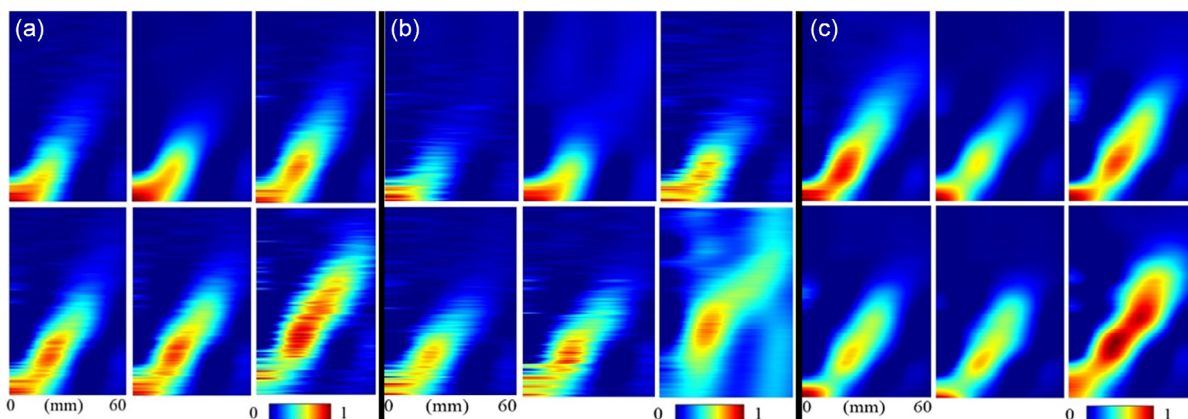


Figure 5. Abel deconvolution of a) OH*, b) NH*, and c) NH₂* intensity profiles from 0.70 to 1.20φ in increments of 0.10φ, from left-top corner to right-bottom corner. Nozzle: NIK17. Arbitrary units.

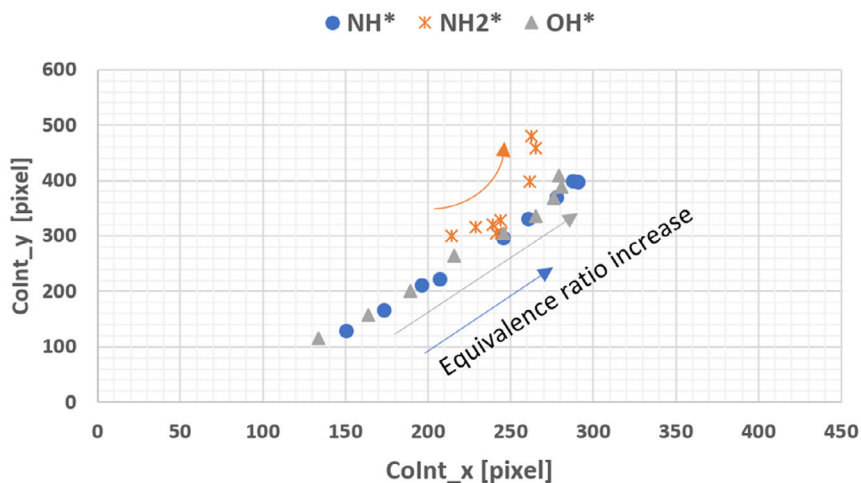


Figure 6. Centers of intensity of all intensity profiles for MK1. The arrow shows the movement of the CoI for each case. Units in pixels.

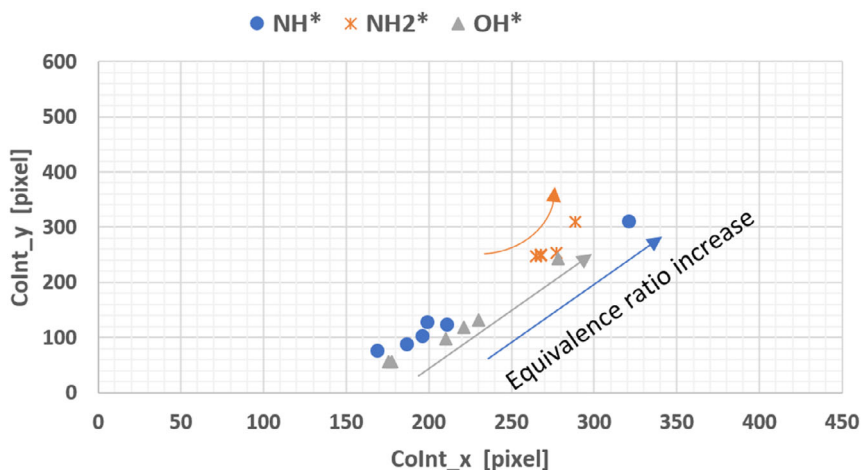


Figure 7. Centers of intensity of all intensity profiles for NIK17. The arrow shows the movement of the CoI for each case. Units in pixels.

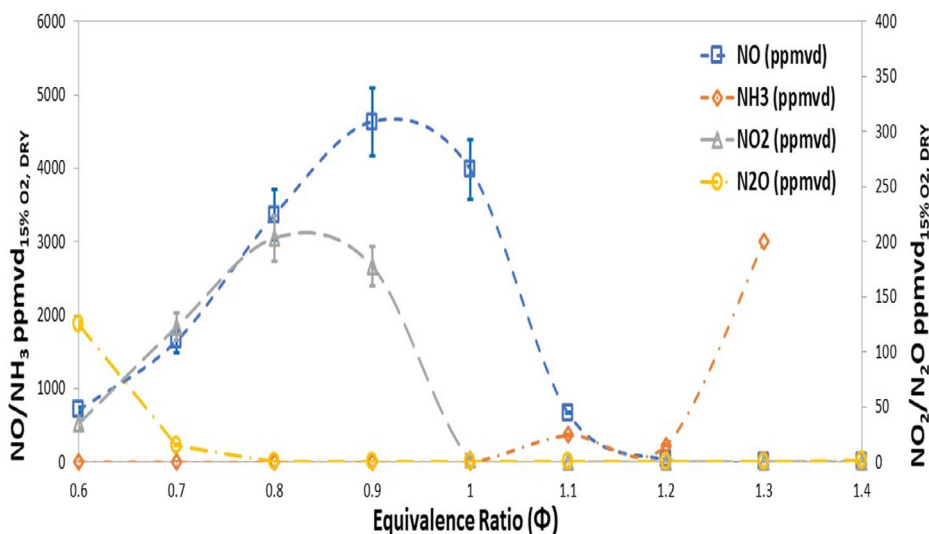


Figure 8. NO_x and unburned ammonia emissions at various equivalence ratios. Ammonia emissions after 1.3 ϕ were outside of the measurement range of the emissions analyzer.

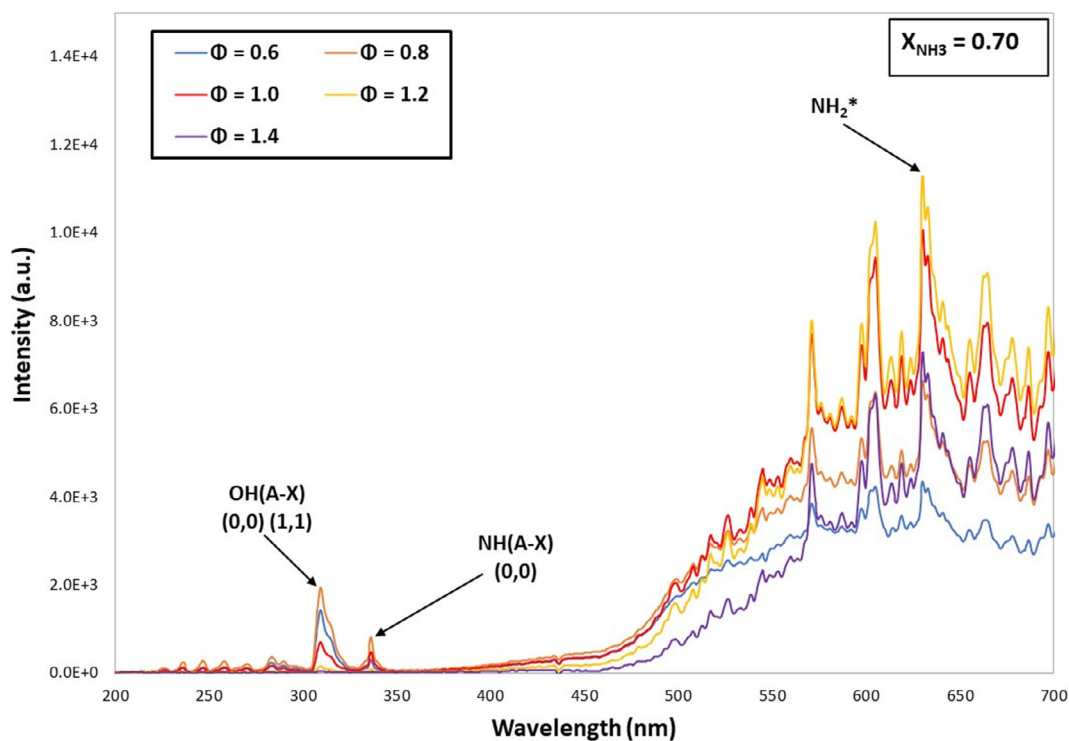


Figure 9. Spectral analysis at various equivalence ratios. NH₂* peaks at 1.2 ϕ .

production of NH₂* remains more homogeneously spread across conditions compared to NH* and OH*. The uplifted position of NH₂* can also be a precedent to the reduced NO production under rich conditions, where the postcombustion zone plays the most important role in NO abatement under oxygen-depleted conditions, as demonstrated by others^[24] via CHEMKIN analyses.

Results show a linear correlation between OH* and NH* signals at various equivalence ratios. It was observed that equivalence ratios from 0.7 to 1.1 show very close connection and a similar trend between both radicals using both nozzles. This is not surprising, as most NH* production is consequence of the reaction NH₂ + OH → NH + H₂O, as documented elsewhere.^[27] NH* and OH* show in both geometries a pattern that

follows a linear regression with a trendline of the form $\alpha X - \beta$ (with $R^2 > 0.97$), being α and β determined by the swirl nozzle geometry and swirl intensity. However, and still not understood, the trends of both radicals swap between conditions, with NH^* being more angled with respect to the X axis than OH^* for MK1, and vice versa for NIK17. Initially, considerations are given to the change in recirculation zones between cases, with NIK17 producing a stronger external recirculation zone compared to MK1. The effect is conceived to enhance anchoring and increase post-combustion reactions, which seems to be achieved (in case this is the reason for the shift in slopes).

However, amidogen (NH_2) shows a more distributed trend. As in the previous reactions, OH radicals produced at the nozzle outlet start interacting with NH_2 to form NH. Under lean conditions, the radicals are quickly formed and consumed, giving rise to a highly localized OH^*/NH^* trend close to the burner. Under those same conditions, further OH and H radicals at the root of the flame interact with NH, hence forming HNO that precedes the formation of NO emissions. Amidogen appears to be present passed this point, potentially recombining with O to form NO via the reaction $\text{NH}_2 + \text{O} \rightarrow \text{HNO} + \text{H}$. The reaction contributes to the total of NO emissions under lean conditions described later. Further, NO emissions from the root and largely available O overwhelm the NH_2 traces at low equivalence ratios, minimizing DeNOxing processes. As the equivalence ratio increases, the location of the flame also moves outward with the production of OH^*/NH^* following this uplifting behavior. However, the CoI of NH_2^* remains anchored, enabling the recombination of recently formed NO with NH_2 via $\text{NO} + \text{NH}_2 \rightarrow \text{H}_2\text{O} + \text{N}_2$. Different from the lean case, where NH_2 increases its reactivity with O radicals, rich conditions ensure that the enhanced NH_2^* zone immediately interacts with NO species in the absence of oxygen, critically DeNOxing these combustion cases. Trends are more complex for amidogen, which denotes a cubic regression.

The latter seems to be also a phenomenon directly linked to the higher O_2 which shows a significant reaction increase under very lean conditions,^[28] producing HNO, H, and even $\text{N}_2\text{O}^{[29]}$ (molecule that has been demonstrated to be highly produced under these very lean regimes^[30] and that also is sensitive to NH_2 formation in OH rich fields^[24]). As for the position of OH^*/NH^* , the higher location of these traces at higher equivalence ratios can be linked to the depleted OH at the core of the flame, which would be consumed by NH_2 in a more distributed way (i.e., evidenced by the highly diffused image of NH^* under rich conditions difficult to obtain).

Different to the latter, NH_2^* starts moving away from the center of the combustion field (where a large recirculation zone is expected to coexist with the shearing flow.^[31,32] Lifted and in closer position to the recirculation zones, NH_2^* shows stronger intensity signals (i.e., no noise) while denoting an extension toward the burner outlet where neither OH^* nor NH^* appear. It is believed that this effect is a consequence of the production of NH_2 by OH remnants in the flow field, see Figure 3, while the recombination of this NH_2 does not take place via $\text{NH}_2 \rightarrow \text{HNO}$ paths, but instead, it increases its recombination with NO through the reaction $\text{NH}_2 + \text{NO} \rightarrow \text{N}_2 + \text{H}_2\text{O}$, as previously mentioned. The latter is the reaction that engineers and researchers currently try to maximize, as this will deliver clean ammonia

combustion without NOx, ammonia slip, or other unwanted pollutants.

Figure 7, using NIK17 Coanda nozzle, shows a similar story to the one produced by MK1. Close to the burner, OH^* and NH^* species are noticeable, while NH_2^* CoI remains anchored further downstream the nozzle outlet. Although not enough points are available to define the correct trend for the NH_2^* behavior—which is anchored with a slight movement at 1.2 equivalence ratio—it is clear that the CoI is not as distributed as that of OH^* and NH^* , which follow a linear trend as in MK1. These results show that trends of these species are neither dependent on nozzle geometry nor power (at least under low power conditions). To what extent swirl strength or larger power ratios affect these results is still to be confirmed in future works.

Experimental results from the emissions analyses done on MK1, Figure 8, denote how NOx has a critical decay under these high equivalence ratio conditions, with values that reach 0 ppm. Although NH_3 starts increasing, there is a region between 1.0 and 1.20ϕ that shows the lowest emission profiles among all cases. Passing that point, unburned ammonia becomes a critical issue. However, the effect is understandable since ammonia is not being oxidized as most OH has been depleted from the combustion field. Similarly, spectral data, Figure 9, show an increase in the intensity of wavelengths between 622 and 642 nm (NH_2^*)^[33–36] at higher ϕ and up to 1.2ϕ , while there is an acute reduction of intensity within the ranges of 303–326 nm (OH^*) and 335–346 nm (NH^*),^[20] confirming the previous assertions and denoting how the lack of OH radicals will impact on oxidation and further production of NH_2 species. These trends replicate the works from others, providing the backup argument as in the previous paragraphs.

Therefore, these works show how both the relocation of NH_2^* closer to the center of the flow field—where potentially large NO emissions are recirculated—and dislocation of species lead to better emissions performance for the use of this blend. Further work on the analysis of other excited radicals such as H^* , O^* , and N^* would provide enough information for designers to not only determine regions of interest, but also to predict the formation of reacting zones according to equivalence ratio. According to Guiberti et al.^[28] who trained a machine learning-based regression algorithm using chemiluminescence data, the recognition of these intensities could be used for flame control purposes, while the accurate location of radicals could serve to develop critically needed emissions control strategies with relatively affordable equipment.

One of the outcomes of this study is that both OH^* and NH^* are in higher concentration close to the nozzle at lean conditions, while NH_2^* mostly concentrates further downstream of the nozzle with a slight displacement toward the sides of the flame confinement as equivalence ratio increases. As depicted with NIK17, the trend follows similar patterns. Also, it has been shown how the presence of OH^* and NH^* radicals changes from a location next to the burner to places higher up in the field as equivalence ratio is reduced, hence depicting the impact on these species as oxygen content changes. This factor, well known, has been poorly analyzed across the flame through experimental campaigns, hence requiring a study like the one presented in this work. Furthermore, the results show that NH_2 , a molecule with high value for NOx abatement, tends to be always localized further

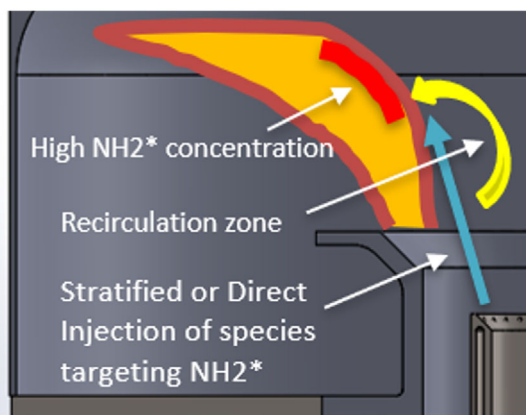


Figure 10. Visual aid showing how the method could be used to target excited species (e.g., NH_2^*) when their location is known. This can support emissions abatement with higher flame stability.

downstream the nozzle irrespective of the burner geometry. Since engineers and developers need to address the issue of NO_x in ammonia combustion systems, the use of excited radical chemiluminescence can be a method to target NH_2 high-concentration zones, and via stratification or direct injection of other species (i.e., NO , H_2O , etc.) to these areas enhance the reduction of pollutants by stopping the decay of amidogen into NH and its subsequent radicals and species (i.e., HNO and NO). The method enables to determine the best locations where to target OH , NH , and NH_2 to maximize the reaction of the molecules, **Figure 10**.

4. Conclusion

The work shows chemiluminescence analyses of an ammonia/hydrogen blend that has been proposed as one of the most stable due to its flame features. To determine the change in reactivity and location of radicals, centers of intensity maps were determined for three critical radicals formed during the oxidation of ammonia (OH^* , NH^* , and NH_2^*). The study depicts the need to properly acknowledge the location of these reaction fields, as the interaction between radicals will lead to the production or consumption of emissions such as NO . Overall, it was observed that: 1) Radical formation tends to change along the field depending on equivalence ratio; 2) Nozzle shape and (low value) power did not change the fundamental trends of these emissions and their appearance across the field, although other relevant parameters such as swirl strength need to be evaluated further; 3) Consistent trends show a flame that starts close to the burner outlet, then is lifted, to eventually split the CoI of OH^* , NH^* , and NH_2^* radicals, dislocating the interaction between species; 4) For OH^* and NH^* , a linear trend of the type $\alpha X\text{-}\beta$ was observed, while NH_2^* fits to cubic regressions; 5) Flame anchoring mechanisms, directly linked to the geometry of the combustor, can have a direct impact on the slope of OH^* and NH^* , a point of further research; 6) NH_2^* appears to be anchored at the core of the flame, a feature that can be exploited to maximize the use of the radical; 7) Trends can be determined via relatively

simple chemiluminescence experimentation, providing a tool for designers to target any of these species with the capacity of predicting where their highest concentration will be located; and 8) Knowledge of these locations will serve modelers for validation purposes, and designers to enhance combustion stability and pollutants mitigation.

Acknowledgements

Cardiff University acknowledges the support from ESPRC through the program SAFE-Pilot AGT (EP/T009314/1). The authors also want to thank Mr. Malcolm Seaborn for his support in the setup of the experimental rig. The authors are grateful to the IEA Combustion Technology Collaboration Program for providing a framework for discussions which influenced this article.

Conflict of Interest

The authors declare no conflict of interest.

Data Availability Statement

Information on the data underpinning the results presented here, including how to access them, can be found in the Cardiff University data catalog at <http://doi.org/10.17035/cardiff.27605553>.

Keywords

ammonia, combustion, emissions, excited radicals, net zero fuels

Received: July 22, 2024
Revised: October 25, 2024
Published online:

- [1] A. Valera-Medina, H. Xiao, M. Owen-Jones, W. I. F. David, P. J. Bowen, *Prog. Energy Combust. Sci.* **2018**, *69*, 63.
- [2] Hydrogen Council, in *Hydrogen Insights*, **2021**. Available online: -- <https://hydrogencouncil.com/en/hydrogen-insights-2021/> [Accessed 11.06.23]
- [3] F. J. Verkamp, J. R. Williams, *Symp. Int. Combust.* **1967**, *11*, 985.
- [4] D. T. Pratt, in *Performance of Ammonia-Fired Gas-Turbine Combustors*, DTIC Document, USA **1967**.
- [5] H. Newhall, E. Starkman, in *Theoretical Performance of Ammonia as a Gas Turbine Fuel*, JSTORSAE Technical Paper 660768, **1966**.
- [6] K. Aika, H. Kobayashi, in *CO₂ Free Ammonia as an Energy Carrier*, Springer, Singapore **2023**.
- [7] J. O'Connor, B. Noble, T. Lieuwen, in *Renewable Fuels: Sources, Conversion, and Utilization*, Cambridge University Press, Cambridge, UK **2022**.
- [8] D. Chen, J. Li, X. Li, Y. Guo, H. Huang, N. Kobayashi, *Int. J. Hydrogen Energy* **2024**, *52*, 1370.
- [9] M. O. Viguera-Zúñiga, D.-C. Tejada, S. Mashruk, M. Kovaleva, C. L. Ordóñez-Romero, A. Valera-Medina, *Energies* **2021**, *14*, 6624.
- [10] S. Mashruk, M. Kovaleva, A. Alnasif, C. T. Chong, A. Hayakawa, E. C. Okafor, A. Valera-Medina, *Energy* **2022**, *260*, 125183.
- [11] S. Mashruk, A. Alnasif, C. Yu, J. Thatcher, J. Rudman, L. Peronski, C. Meng-Choung, A. Valera-Medina, *J. Ammonia Energy* **2023**, *1*, 21.
- [12] A. M. Elbaz, S. Wang, T. F. Guibert, W. L. Roberts, *Fuel Commun.* **2022**, *10*, 100053.

- [13] A. Stagni, C. Cavallotti, S. Arunthanayothin, Y. Song, O. Herbinet, F. Battin-Leclerc, T. Faravelli, *React. Chem. Eng.* **2020**, *5*, 696.
- [14] M. Keller, M. Koshi, J. Otomo, H. Iwasaki, T. Mitsumori, K. Yamada, *Energy* **2020**, *194*, 116894.
- [15] P. Glarborg, J. A. Miller, B. Ruscic, S. J. Klippenstein, *Prog. Energy Combust. Sci.* **2018**, *67*, 31.
- [16] S. Mashruk, S. E. Zitouni, P. Brequigny, C. Mounaim-Rousselle, A. Valera-Medina, *Int. J. Hydrogen Energy* **2022**, *47*, 41170.
- [17] A. Karan, G. Dayma, C. Chauveau, F. Halter, *J. Ammonia Energy* **2023**, *1*, 118.
- [18] M. Suarez, M. K. Hay, K. Naude, W. Kulatilaka, in *AIAA SciTech Forum*, Orlando, FL **2024**.
- [19] X. Zhu, A. A. Khateeb, W. L. Roberts, T. F. Guiberti, *Combust. Flame* **2021**, *231*, 111508.
- [20] S. Mashruk, X. Zhu, W. L. Roberts, T. F. Guiberti, A. Valera-Medina, *Proc. Combust. Inst.* **2023**, *39*, 1415.
- [21] M. M. Kamal, *Energy* **2020**, *192*, 116485.
- [22] A. A. Konnov, *Part 1. Combust. Flame* **2023**, *253*, 112788.
- [23] D. Pugh, P. Bowen, R. Navaratne, B. Goktepe, A. Giles, A. Valera-Medina, S. Morris, R. Vivoli, *J. Eng. Gas Turbines Power* **2024**, *146*, 061006.
- [24] W. Weng, M. Aldén, Z. Li, *Proc. Combust. Inst.* **2023**, *39*, 4327.
- [25] J. Davies, L. Mazzotta, D. Sato, S. Mashruk, D. Pugh, D. Borello, A. Valera-Medina, in *Ceramics and Ceramic Composites; Coal, Biomass, Hydrogen, and Alternative Fuels*, American Society of Mechanical Engineers, London, UK **2024**.
- [26] J. Zhang, W. Jing, T. Fang, *Fuel* **2012**, *99*, 226.
- [27] A. Alnasif, S. Mashruk, M. Kovaleva, P. Wang, A. Valera-Medina, *Carbon Neutrality* **2022**, *1*, 24.
- [28] J. A. Miller, C. T. Bowman, *Prog. Energy Combust. Sci.* **1989**, *15*, 287.
- [29] C. Duynslaegher, F. Contino, J. Vandooren, H. Jeanmart, *Combust. Flame* **2012**, *159*, 2799.
- [30] S. Mashruk, E. C. Okafor, M. Kovaleva, A. Alnasif, D. Pugh, A. Hayakawa, A. Valera-Medina, *Combust. Flame* **2022**, *244*, 112299.
- [31] R. Sharma, M. Kumar, *J. Appl. Fluid Mech.* **2023**, *16*, 549.
- [32] N. Syred, *Prog. Energy Combust. Sci.* **2006**, *32*, 93.
- [33] A. Hayakawa, T. Goto, R. Mimoto, T. Kudo, H. Kobayashi, *Mech. Eng. J.* **2015**, *2*, 14-00402.
- [34] T. F. Guiberti, N. N. Shohdy, S. Cardona, X. Zhu, L. Selle, C. J. Lapeyre, *Appl. Energy Combust. Sci.* **2023**, *16*, 100212.
- [35] J. Li, H. Huang, N. Kobayashi, Y. Nagai, *Int. J. Energy Res.* **2014**, *38*, 1214.
- [36] J. H. Kim, J. H. Song, J. W. Ku, Y. H. Kim, O. C. Kwon, *Int. J. Hydrogen Energy* **2024**, *49*, 1075.